Vietnam Journal of Science and Technology ***61*** *(3) (2023) 620-630*

doi:10.15625/2525-2518/18064

Efficient and reliable detection of rhodamine B using SERS from silver-decorated nanoporous silicon photonic crystal

Do Thuy Chi[1], Nguyen Thuy Van[2, 3, *], Vu Duc Chinh[2, 3], Hoang Thi Hong Cam[4], Vilaysak Sayyasone[1], Pham Thanh Binh[2, 3], Bui Huy[2, 3], Pham Van Hoi[2, 3]

[1]*Thai Nguyen University of Education, Thai Nguyen University, 20 Luong Ngoc Quyen, Thai Nguyen City, Thai Nguyen, Viet Nam*

[2]*Institute of Materials Science, Vietnam Academy of Science and Technology, 18 Hoang Quoc Viet, Cau Giay, Ha Noi, Viet Nam*

[3]*Graduate University of Science and Technology, Vietnam Academy of Science and Technology, 18 Hoang Quoc Viet, Cau Giay, Ha Noi, Viet Nam*

[4]*University of Science and Technology of Hanoi, Vietnam Academy of Science and Technology, 18 Hoang Quoc Viet, Cau Giay, Ha Noi, Viet Nam*

[*]Emails: *vannt@ims.vast.ac.vn*

Received: 6 February 2023; Accepted for publication: 1 June 2023

Abstract. Porous silicon photonic crystal (PSi PhC) decorated with silver nanoparticles (AgNPs) is shown to provide a new substrate for the improvement of SERS. AgNPs are obtained through immersion of PSi PhC samples in $AgNO_3$ solutions and successive thermal annealing. The nanocomposite material generated by adding AgNPs inside the silicon nanoscale pores, integrates the ability of metal surfaces to amplify Raman scattering signals and an enlarged surface area. Besides, PhC structure formed by multilayer PSi increases interaction time of light and matter of the multilayer structure. The experimental results show that the AgNPs-decorated PSi PhC has the largest Raman intensity in comparison with other SERS substrates based on Si. The enhancement of Raman signals also reduces the threshold of the detection down to below 10^{-10} M. The analytical enhancement factor of AgNPs/PSi PhC SERS substrate for the detection of Rhodamine B (RhB) reaches 10^{10}. This proposed AgNPs/PSi PhC SERS substrate could serve as a potential candidate for detecting RhB in foodstuffs at very low concentrations.

Keywords: porous silicon, photonic crystal, silver nanopaticles, SERS, Rhodamine B.

Classification numbers: 2.1.3, 2.5.1, 2.5.2.

1. INTRODUCTION

Rhodamine B (RhB), a bright pink synthetic fluorescent dye, widely used in many industries such as cosmetic, textile, medical as well as paper production [1]. Due to its low cost, high effectiveness and excellent stability of color, RhB is frequently used as the colorant in various foods, including chili powder, chili oil, preserved plums, sausage and sweets [2].

However, following a thorough safety evaluation, it is reported about its harmful effects on human health such as irritation to the skin, eyes, gastrointestinal tract as well as respiratory tract, and even causing carcinogenicity [3]. Therefore, it is an urgent need to develop a reliable and cost-effective method to sensitively detect RhB. There are various analytical techniques for detecting RhB, such as high performance liquid chromatography (HPLC) [4], spectrophotometry [5], UV-Vis spectrometry [6], enzyme-linked immunosorbent assays (ELISA) [7]. However, these methods generally suffer from needing complex pretreatment, a long preparation time and expensive equipment, making them difficult to use for the in-situ analysis. In recent years, the surface-enhanced Raman scattering (SERS) technique has gained great interest from researchers in many fields like food, materials and medicine [8] because of its high sensitivity and molecular specificity. SERS is an easy, simple and rapid method, which is capable of detecting and identifying a small number of molecules, reaching even the ultimate limit of detection, single-molecule detection [9].

It is well-known that the capacity of SERS is characterized by its ability to enlarge the enhancement Raman signal [10] which depends on various factors, including the substrate, the sensing mechanism and other environmental influences. One way to improve sensing performance is to use nano-structure substrates which afford high specific surface area, good adsorption properties. The sensitive substrates used in SERS sensors are porous structures [11] and photonic crystal (PhC) [12, 13]. Among those, one type of porous substrates that have attracted much interest because of its unique optical and physical characteristics for sensor applications, is porous silicon (PSi)-based device. The most attractive feature of PSi for SERS active substrates is its compatibility with the biomolecules, as devices based on PSi can be easily composited with other materials after the multi-functional modification. The main reason for choosing PSi nano-materials is that PSi is not only used as a mechanical support for the formation of the nanostructured metal film, but also as a reducing agent. PSi deposited with noble metals (Au, Ag, Pt…) has been reported to obtain excellent SERS performance [14]. However, most research focuses on the main SERS effect of single-layer PSi structures; on the other hand, sensors based on the SERS effect of PSi PhCs have been rarely reported. The PhC structure has strength in improving the Raman scattering efficiency of the analyte [15] owing to its long light-matter interaction time [16] and the total internal reflection [13]. PSi PhCs can be facilely prepared by anodic electrochemical etching, which is simple, cheap, controllable, repeatable and compatible with modern silicon technology [17].

In this report, effective SERS substrates were fabricated by infiltrating AgNPs into the porous network of PSi PhC structure using the immersion of PSi PhC samples in $AgNO_3$ solutions and successive thermal annealing for qualitative identification and quantitative determination of very low concentration of RhB. The prepared SERS substrate can provide high analytical enhancement factor of detecting RhB (below 10^{-10} M) up to 10^{10} and can be used as an efficient probe in detection of RhB in foodstuffs.

2. MATERIALS AND METHODS

2.1. Materials

Monocrystalline silicon wafers used in this work were single-side polished p-type, boron-doped, with typical resistivity 0.002 - 0.004 Ωcm, (100) orientations and 500 - 550 µm thickness, obtained from CrysTec GmbH, Germany. Hydrofluoric acid 48 wt% (HF, Merck Millipore) was diluted with absolute ethanol (99.9 %, Merck Millipore) to make the electrolyte

solutions in a volume ratio of 1:2. Silver nitrate ($AgNO_3$, ≥ 99.0 %) was dissolved in deionized water to prepare solution of 0.1 M for synthesis of silver nanoparticles. Rhodamine B (RhB) was purchased from Sigma-Aldrich and dissolved in deionized water to obtain the standard stock 10^{-2} M analyte solutions. Different concentrations (from 10^{-5} M to 10^{-12} M) were obtained by successive dilution of stock solutions with water.

2.2. Methods

Porous silicon layers were fabricated by an electrochemical method in a process as presented in our previous work [18]. The 50 mA/cm^2 current density was used for etching the single-layer PSi sample and the low refractive index layers of PSi PhC. The same porosities of these two structure samples ensure that the same number of probe molecules inside the PSi. Current densities of 50 mA/cm^2 for 3 s and 15 mA/cm^2 for 6 s were applied alternately for the fabrication of PSi PhC structure. The total etching time was 12 cycles. After etching, the samples were washed with deionized water and dried under steam of nitrogen gas.

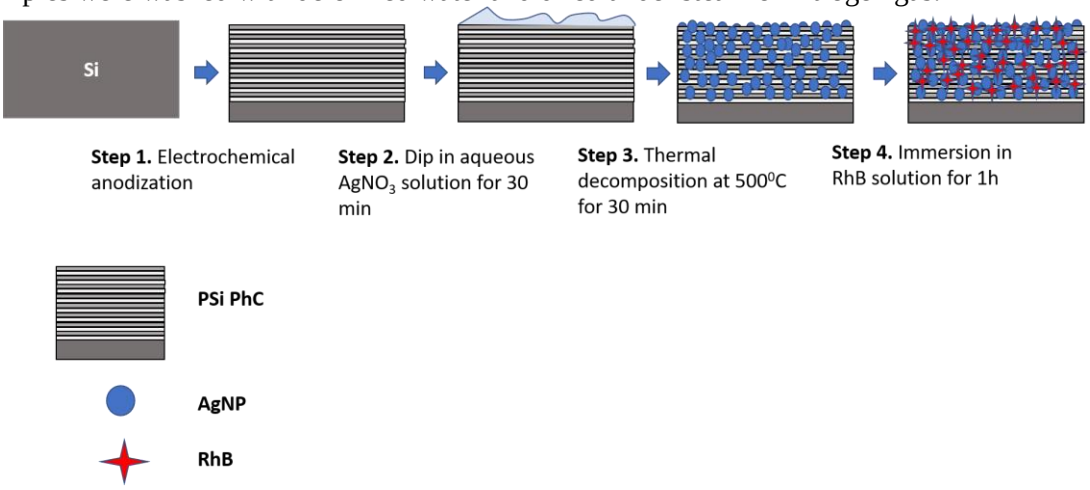

Figure 1. Preparation process of AgNPs/PSi PhC substrate.

The fabrication of SERS substrates involves four steps, beginning with the anodization of PSi PhC (step 1), as depicted in Figure 1. Next, the fresh PSi samples were immersed into aqueous $AgNO_3$ solution for 30 min to completely wet the pores (Figure 1, step 2). After the dip coating synthesis, the substrates were heated to 500 ^oC in an ambient pressure furnace in order to thermally decompose $AgNO_3$ salt into Ag [19, 20]. This process permitted a total decomposition of silver nitrate in metallic silver then Ag filled deeply the silicon pores. Silver-embedded nanoporous silicon substrates used for SERS were immersed in RhB solution for 1 h. The samples were naturally dried in the air.

The reflectance spectra of samples were characterized by a spectrometer (USB-4000, Ocean Optics) and a halogen light source (HL-2000 Ocean Optics). Their structure and morphology were examined by the field emission scanning electron microscope (FESEM, Hitachi S-4800, Japan) and energy dispersive X-ray spectroscopy (EDX) integrated in the FESEM system. Raman spectra were measured by a Raman microscope system (Horiba Scientific LabRAM HR Evolution), equipped with laser of 532 nm wavelength emission for excitation. Every Raman spectrum in this work presents the result of averaging the seven measurements at different positions on the same sample.

3. RESULTS AND DISCUSSION

3.1. Reflectance and SEM characteristics of PSi PhC sample

Figure 2a shows the SEM image of the surface of PSi PhC structure. Top-view observation reveals that the PSi PhC has a uniform distribution of pores with a diameter of 15 to 55 nm, estimated from the SEM image. The cross-section SEM image, as shown in Figure 2b, presents the hierarchy of 12 cycles and that the thickness of PSi was around 1.2 µm. The layers with high and low porosities were formed by anodic electrochemical etching using large and small current densities, respectively. Figure 2c depicts the reflectance spectrum of PSi PhC structure, the center wavelength of the band-gap is at 680 nm which is suitable to the excitation wavelength of laser. The arrangement of the band-gap of the PhC is longer than the excitation wavelength, i.e., 532 nm and it is expected to achieve high Raman scattering because the intensity of Stokes scattering (or anti-Stokes scattering) is proportional to the transmission coefficient [16].

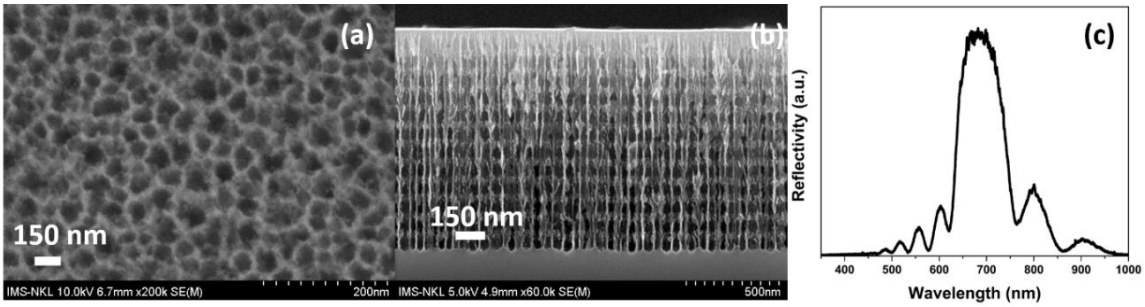

Figure 2. SEM images of PSi PhC: (a) top view of PSi PhC; (b) cross-section view of PSi PhC, and (c) reflectance spectrum of PSi PhC structure.

3.2. Morphology of AgNPs/PSi PhCs

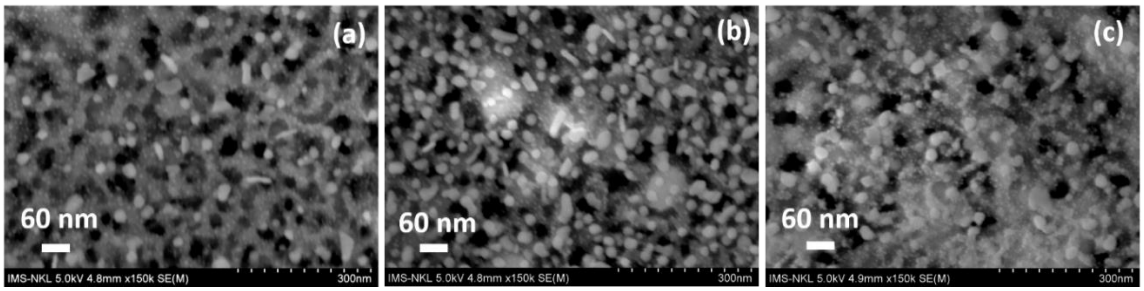

Figure 3. Scanning electron microscope (SEM) images of surface topographies of AgNPs decorated PSi PhC with different concentrations of $AgNO_3$ solution of: (a) 10^{-2} M, (b) 10^{-1} M, and (c) 1 M.

Figure 3 shows the SEM images of the AgNPs decorated PSi PhC obtained with different soaking concentration of $AgNO_3$ solution 10^{-2} M, 10^{-1} M and 1 M in the same duration of 30 minutes. As the concentration of $AgNO_3$ increases, the number of AgNPs increases and the gap between the NPs reduces as shown in Figures 3(a, b). Besides, when the concentration of $AgNO_3$ solution is more than 10^{-1} M, many overlaps between AgNPs apprear to generate clusters or islands of Ag on the surface of PSi as seen in Figure 3c.

Figure 4a presents the SEM cross-sectional images of the AgNPs which diffuse down into

silicon pore depths inside PSi PhC structures. It can be observed that the AgNPs were evenly distributed inside the nanopores. This even distribution results from using successive thermal annealing method. Figure 4b shows the reflectance spectrum of PSi PhC structure before and after infiltration of AgNPs with concentration of 10^{-1} M $AgNO_3$. The infiltrated metal NPs not only enhances the optical absorption of photonic and plasmonic devices [21, 22] but also breaks Bragg condition of PhCs. As a result, this leads to disappear the photonic band-gap. The existence of AgNPs deposited inside PSi PhC structures measured by the EDX is demonstrated in Figure 4c. The appearance of the Si and O elements is obvious in EDX spectra because of the Si substrate and the oxidation of Si [23, 24].

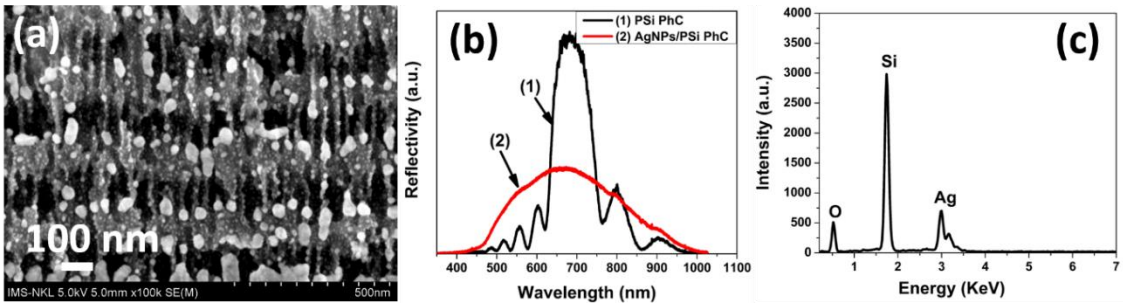

Figure 4. (a) SEM images of infiltrated AgNPs inside the nanopores of PSi PhC; (b) reflectance spectrum of PSi PhC before and after infiltration of AgNPs, and (c) EDX analysis of AgNPs inside the nanopores of PSi PhC.

3.3. The SERS activity of the substrates

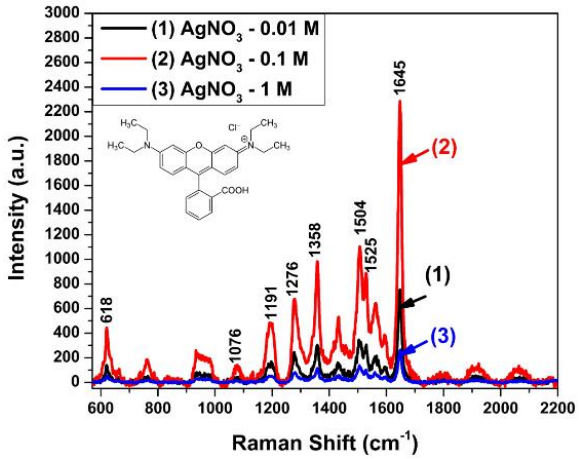

Figure 5. Raman spectra of RhB adsorbed on SERS substrates with PSi PhCs immersed in $AgNO_3$ solution (0.01 M, 0.1 M and 1 M). Inset: Molecular structure of RhB.

Figure 5 illustrates comparative SERS intensities of RhB molecules (10^{-8} M) obtained on AgNPs/PSi PhC surfaces, where PSi PhCs were immersed in $AgNO_3$ solution (0.01 M, 0.1 M and 1 M) in the same experimental conditions. It is observed that the largest intensity of the Raman signal is achieved at concentration of 0.1 M. This is coincidental with the field enhancement resulting from the size of AgNPs and the distance between particles in Figure 3(a, b) [25]. For the 1 M $AgNO_3$ concentration, the Raman signal of RhB drops because the layer of

AgNPs is too thick which hinders the elesctromagnetic interaction between Si and AgNPs as reported in the literature [12]. In addition, at low concentration of $AgNO_3$, the distance between AgNPs is quite large which cannot form strong field. Therefore, concentration of $AgNO_3$ solution of 10^{-1} M was used so that the prepared SERS substrates possess the strongest LSPR field. We have noticed the presence of the main vibrational modes of the RhB on the SERS spectra. The Raman band located at 618 cm^{-1} is assigned to the xanthene ring puckering mode [26] and the other peaks in the region from 1000 to 1700 cm^{-1} are related to C-C, C-H and C=C [27]. The characteristic Raman peaks of RhB are marked in the spectra corresponding to assignments of the bands listed in Table 1. The intensity of the peak at 1645 cm^{-1} was chosen as the parameter to characterize the SERS signal.

Table 1. Primary characteristic Raman peaks of RhB corresponding to their assignments [26, 27].

RhB Raman shift (cm^{-1})	Assignment
618	Xanthene ring puckering
1076	C–C bridge band stretching and aromatic C–H bending
1191	C-H in plane bending
1276	Aromatic C-C stretch
1358	Aromatic C-C stretch
1504	Aromatic C-H bending
1525	Aromatic C-H bending
1645	Aromatic C-C bending and C=C stretching

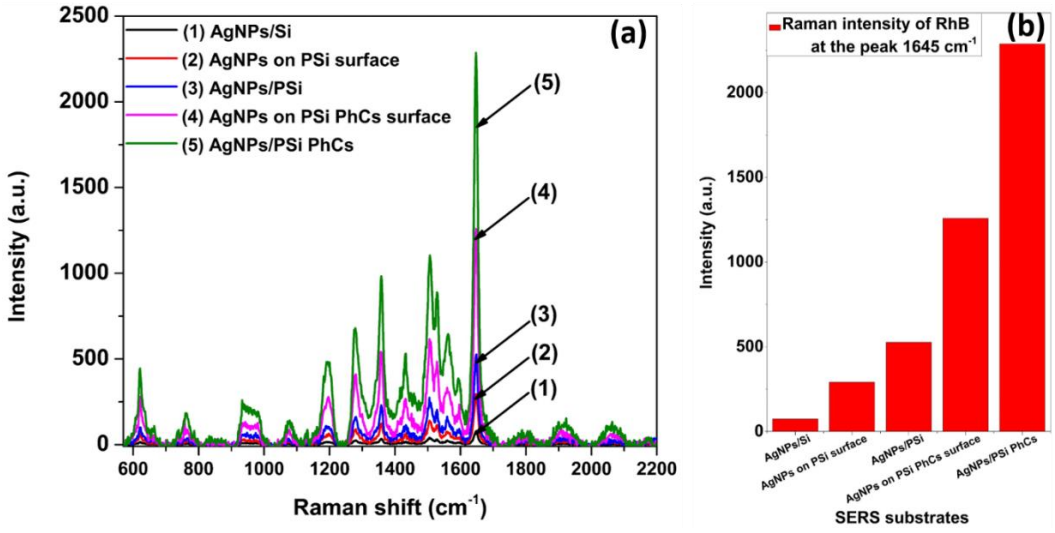

Figure 6. (a) The Raman spectra of RhB and (b) the Raman intensity at the peak 1645 cm^{-1} adsorbed on different SERS substrates.

In order to evaluate the behavior of AgNPs decorated inside the PSi PhC, the SERS intensities of RhB molecules (10^{-8} M) were measured on different SERS substrates including AgNPs on Si surface (curve 1), on PSi surface (curve 2), embedded into single-layer PSi pores

(curve 3), on PSi PhC surface (curve 4) and embedded into PSi PhC pores (curve 5), respectively, as shown in Figure 6a. The SERS intensities gradually increase from the SERS substrate fabricated using AgNPs on Si surface to AgNPs embedded into PSi PhC pores. Figure 6b focuses on the Raman intensities of these SERS substrates at 1645 cm^{-1} peak, which clearly shows this observation. The SERS substrate fabricated from AgNPs embedded into PSi PhC pores has largest intensity because of its unique structure. The Raman intensity is enhanced due to the roughness of the PSi [28]. Besides, the light-matter interaction increases in PSi PhC compared with the single PSi layer [29, 30]. Furthermore, the AgNP-embedded into PSi PhC pores creates high surface-to-volume ratio, i.e., large surface area, which enhances the Raman signal [31].

Figure 7a presents the SERS signals of RhB excited at 532 nm wavelength with varying concentration from 10^{-12} to 10^{-5} M adsorbed on the AgNPs/PSi PhC substrates. It is shown that SERS signal is attained at all RhB concentrations of the range from 10^{-11} to 10^{-5} M and the basic SERS signals of RhB molecules can still be identified at the extremely low concentration of 10^{-10} M. Therefore, it can be concluded that AgNPs/PSi PhC structures can be applied to detect colorless RhB dye (below 10^{-7} M) in food. A linear dependence between logarithmic concentration of RhB and the peak heights at 1645 cm^{-1} was observed for SERS substrates based on AgNPs/PSi PhC (Figure 7b). In addition, the results show a good linearity with great reliability (R^2 = 0.99) over a wide concentration range. To quantitatively estimate the Raman activity of AgNPs/PSi PhC substrate, we calculate the analytical enhancement factor (AEF) according to the formula [32]:

$$AEF = \frac{I_{SERS}}{I_R} \times \frac{C_R}{C_{SERS}} \quad (1)$$

where I_{SERS} and I_R correspond to the Raman intensities of RhB on the AgNPs/PSi PhC and PSi PhC, respectively. C_{SERS} and C_R refer to the molar concentration of RhB on the AgNPs/PSi PhC (10^{-10} M) and PSi PhC (1 M), respectively. The AEF of SERS was estimated to be 10^{10} at the Raman peak of 1645 cm^{-1}, relatively high in SERS application. Table 2 shows the comparison of EF for detecting RhB of different SERS substrates. The AgNPs/PSi PhC SERS substrate exhibits a high EF of RhB up to 10^{10}, which indicates a good SERS substrate for sensing applications.

Table 2. Comparison of enhancement factor of different SERS substrates for detecting RhB.

SERS substrates	EF
Filter paper decorated AgNPs	4×10^7 [33]
AgNPs/rGO	2×10^7 [34]
Black Phosphorous flakes	~ 10^6 [35]
Silver nanowires	4.01×10^6 [36]
AgNPs/PSi PhC	10^{10} [this work]

The stability and the reproducibility of the SERS substrate from AgNPs/PSi PhC were investigated as follows. We prepared 6 samples under the same fabrication protocol. Then, one sample was used to adsorb RhB 10^{-8} M directly and other samples were stored in the vacuum desiccator to avoid light condition within 10, 20, 30, 40 and 60 days. These 6 tested samples were treated under the same preparation condition to adsorb RhB at 10^{-8} M and the Raman spectra were collected. Figure 8a depicts the Raman intensity of RhB in which the stable Raman

signals were obtained, especially the intensity of the peak at 1645 cm^{-1}. Figure 8b illustrates the reduction of the intensity at 1645 cm^{-1} in concentration of 10^{-8} M RhB detected by AgNPs/PSi PhC by different storage times. After 10 days of storing, the SERS substrate remained almost unchanged which was proved by 99.8 % resembled that of the fresh one. The intensity experienced a reduction to about 87 %, 64 %, 55 % and 34 % by storing in 20, 30, 40 and 60 days, respectively. However, the intensity of RhB was still higher than 50 % after keeping for 40 days. This month-scale life-time of our SERS substrates demonstrates the stable performance and reproducibility this detection technique.

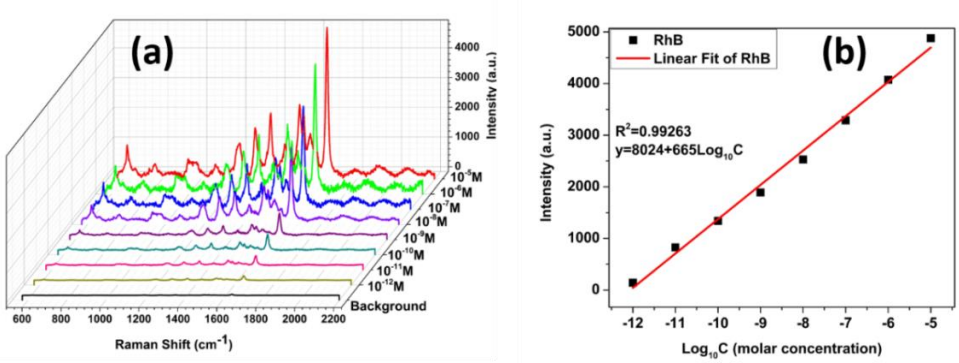

Figure 7. (a) The Raman spectra of RhB solutions with different concentrations ranging from 10^{-5} M to 10^{-12} M and the background curve measured by normal Raman technique from 1 M concentration of RhB and (b) corresponding linear fitting of Raman intensity at 1645 cm^{-1} with logarithmic RhB concentration.

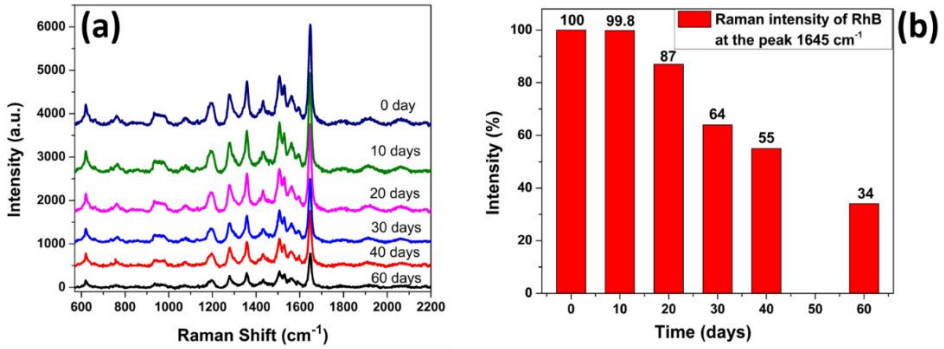

Figure 8. (a) Raman spectra of RhB (10^{-8} M) adsorbed on AgNPs/PSi PhC, and (b) Raman intensity decrease at the peak 1645 cm^{-1} after storing in 0, 10, 20, 30, 40, 60 days.

4. CONCLUSIONS

In this work, AgNPs/PSi PhC SERS substrates were successfully fabricated by a simple, low-cost and efficient method by combining the immersion of PSi PhC into $AgNO_3$ solution with successive thermal annealing. Our proposed substrate can detect RhB at concentration below 10^{-10} M. The fabricated SERS substrates produced a good dynamic linear range of six orders of RhB levels (from 10^{-5} M to 10^{-11} M) with stability and reproducibility. The obtained results demonstrate the potential of using these substrates to detect the presence of RhB in food.

Acknowledgements. This research is funded by Vietnam National Foundation for Science and Technology Development (NAFOSTED) under grant number 103.03-2019.310 and the international cooperation

project between Vietnam Academy of Science and Technology (VAST) and National Academy of Science of Belarus under grant number: QTBY01.02/22-23.

CRediT authorship contribution statement. Do Thuy Chi: Methodology, Investigation. Nguyen Thuy Van: Topic, Manuscript preparation, Methodology, Investigation, Formal analysis, Supervision. Vu Duc Chinh: Formal analysis, Supervision. Hoang Thi Hong Cam: Formal analysis. Vilaysak Sayyasone: Formal analysis. Pham Thanh Binh: Formal analysis. Bui Huy: Supervision. Pham Van Hoi: Supervision.

Declaration of competing interest. The authors declare that they have no known competing financial interests or personal relationships that could have appeared to influence the work reported in this paper.

REFERENCES

1. Al-Buriahi A. K., Al-Gheethi A. A., Kumar P. S., Mohamed R. M. S. R., Yusof H., Alshalif A. F., Khalifa N. A. - Elimination of rhodamine B from textile wastewater using nanoparticle photocatalysts: A review for sustainable approaches, Chemosphere **287** (2022) 132162. https://doi.org/10.1016/j.chemosphere.2021.132162.
2. Huang Y., Wang D., Liu W., Zheng L., Wang Y., Liu X., Fan M., Gong Z. - Rapid screening of rhodamine B in food by hydrogel solid-phase extraction coupled with direct fluorescence detection, Food Chem. **316** (2020) 126378. https://doi.org/10.1016/j.foodchem.2020.126378.
3. Cheng Y. Y. and Tsai T. H. - Pharmacokinetics and Biodistribution of the Illegal Food Colorant Rhodamine B in Rats, J. Agric. Food Chem. **65** (2017) 1078-1085. https://doi.org/10.1021/acs.jafc.6b04975.
4. Gagliardi L., De Orsi D., Cavazzutti G., Multari G., and Tonelli D. - HPLC determination of rhodamine B (C.I. 45170) in cosmetic products, Chromatographia **43** (1996) 76-78. https://doi.org/10.1007/BF02272825.
5. Xiao N., Deng J., Huang K., Ju S., Hu C., and Liang J. - Application of derivative and derivative ratio spectrophotometry to simultaneous trace determination of rhodamine B and rhodamine 6G after dispersive liquid–liquid microextraction, Spectrochim. Acta Part A Mol. Biomol. Spectrosc. **128** (2014) 312-318. https://doi.org/10.1016/j.saa.2014.02.180.
6. Yilmaz E. and Soylak M. - A novel and simple deep eutectic solvent based liquid phase microextraction method for rhodamine B in cosmetic products and water samples prior to its spectrophotometric determination, Spectrochim. Acta Part A Mol. Biomol. Spectrosc **202** (2018) 81-86. https://doi.org/10.1016/j.saa.2018.04.073.
7. Oplatowska M. and Elliott C. T. - Development and validation of rapid disequilibrium enzyme-linked immunosorbent assays for the detection of Methyl Yellow and Rhodamine B dyes in foods, Analyst **136** (2011) 2403-2410. https://doi.org/10.1039/C0AN00934B.
8. Krajczewski J., Ambroziak R., and Kudelski A. - Substrates for Surface-Enhanced Raman Scattering Formed on Nanostructured Non-Metallic Materials: Preparation and Characterization, Nanomaterials **11** (2020) 75. https://doi.org/10.3390/nano11010075.
9. Bandarenka H. V., Girel K. V., Zavatski S. A., Panarin A., and Terekhov S. N. - Progress in the development of SERS-active substrates based on metal-coated porous silicon, Materials (Basel). **11** (2018) 852. https://doi.org/10.3390/ma11050852.
10. Lu Z., Wei W., Yang J., Xu Q., and Hu X. Y. - Improved SERS performance of a silver triangular nanoparticle/TiO 2 nanoarray heterostructure and its application for food

additive detection, New J. Chem. **46** (2022) 7070-7077. https://doi.org/10.1039/D2NJ00388K.

11. Xiang S., Wang X., Pang Y., Ge C., Xu Y., Chen L., Li S., Wang L. - Porous Au/AAO: A simple and feasible SERS substrate for dynamic monitoring and mechanism analysis of DNA oxidation, Appl. Surf. Sci. **606** (2022) 154842. https://doi.org/10.1016/j.apsusc.2022.154842.
12. Zhong F., Wu Z., Guo J., and Jia D. - Porous Silicon Photonic Crystals Coated with Ag Nanoparticles as Efficient Substrates for Detecting Trace Explosives Using SERS, Nanomaterials **8** (2018) 872. https://doi.org/10.3390/nano8110872.
13. Škrabić M., Kosović M., Gotić M., Mikac L., Ivanda M., and Gamulin O. - Near-Infrared Surface-Enhanced Raman Scattering on Silver-Coated Porous Silicon Photonic Crystals, Nanomaterials **9** (2019) 421. https://doi.org/10.3390/nano9030421.
14. Singh N., Shrivastav A. M., Vashistha N., and Abdulhalim I. - 3D plasmonic hot spots network via gold decorated deep micro-porous silicon exhibiting ultrahigh-SERS enhancement with application to explosives detection, Sens. Actuators B Chem. **374** (2023) 132813. https://doi.org/10.1016/j.snb.2022.132813.
15. Lin S., Zhu W., Jin Y., and Crozier K. B. - Surface-Enhanced Raman Scattering with Ag Nanoparticles Optically Trapped by a Photonic Crystal Cavity, Nano Lett. **13** (2013) 559–563. https://doi.org/10.1021/nl304069n.
16. Wang J., Jia Z., and Liu Y. - Improvement of SERS by the Optical Modulation of Photonic Crystal, IEEE Sens. J. **19** (2019) 11221-11227. https://doi.org/10.1109/JSEN.2019.2937092.
17. Ivanov I. I., Skryshevsky V. A., Serdiuk T., and Lysenko V. - Kinetics of adsorption–desorption processes of alcohol molecules in porous silicon Bragg mirror," Sens. Actuators B Chem. **174** (2012) 521-526. https://doi.org/10.1016/j.snb.2012.02.056.
18. Bui H., Pham V. H., Pham V. D., Hoang T. H. C., Pham T. B., Do T. C., Ngo Q. M. and Nguyen T. V. - Determination of low solvent concentration by nano-porous silicon photonic sensors using volatile organic compound method, Environ. Technol. **40** (2019) 3403-3411. https://doi.org/10.1080/09593330.2018.1474268.
19. Giorgis F., Descrovi E., Chiodoni A., Froner E., Scarpa M., Venturello A., Geobaldo F. - Porous silicon as efficient surface enhanced Raman scattering (SERS) substrate, Appl. Surf. Sci. **254** (2008) 7494-7497. https://doi.org/10.1016/j.apsusc.2008.06.029.
20. Novara C., Marta S. D., Virga A., Lamberti A., Angelini A., Chiadò A., Rivolo P., Geobaldo F., Sergo V., Bonifacio A., and Giorgis F. - SERS-Active Ag Nanoparticles on Porous Silicon and PDMS Substrates: A Comparative Study of Uniformity and Raman Efficiency, J. Phys. Chem. C **120** (2016) 16946-16953. https://doi.org/10.1021/acs.jpcc.6b03852.
21. Maiti R., Sinha T. K., Mukherjee S., Adhikari B., and Ray S. K. - Enhanced and Selective Photodetection Using Graphene-Stabilized Hybrid Plasmonic Silver Nanoparticles, Plasmonics **11** (2016) 1297-1304. https://doi.org/10.1007/s11468-015-0175-0.
22. Govorov A. O. and Carmeli I. - Hybrid Structures Composed of Photosynthetic System and Metal Nanoparticles: Plasmon Enhancement Effect, Nano Lett. **7** (2007) 620–625. https://doi.org/10.1021/nl062528t.
23. Len'shin A. S., Kashkarov V. M., Turishchev S. Y., Smirnov M. S., and Domashevskaya E. P. - Effect of natural aging on photoluminescence of porous silicon, Tech. Phys. Lett. **37** (2011) 789–792. https://doi.org/10.1134/S1063785011090124.

24. Sinha S., Piekiel N. W., Smith G. L., and Morris C. J. - Investigating aging effects for porous silicon energetic materials, Combust. Flame **181** (2017) 164-171. https://doi.org/10.1016/ j.combustflame.2017.03.015.
25. Lu G., Wang G., and Li H. - Effect of nanostructured silicon on surface enhanced Raman scattering, RSC Adv. **8** (2018) 6629-6633. https://doi.org/10.1039/C8RA00014J.
26. Yang D., Mircescu N. E., Zhou H., Leopold N., Chiş V., Oltean M., Ying Y, Haisch C. - DFT study and quantitative detection by surface-enhanced Raman scattering (SERS) of ethyl carbamate, J. Raman Spectrosc. **44** (2013) 1491-1496. https://doi.org/10.1002/jrs.4375.
27. Wang J., Luo H., Zhang M., Zu X., Li Z., and Yi G. - Aligned Chemically Etched Silver Nanowire Monolayer as Surface-Enhanced Raman Scattering Substrates, Nanoscale Res. Lett. **12** (2017). 587. https://doi.org/10.1186/s11671-017-2358-4.
28. Dridi H., Haji L., and Moadhen A. - Rough SERS substrate based on gold coated porous silicon layer prepared on the silicon backside surface, Superlattices Microstruct. **104** (2017) 266-270. https://doi.org/10.1016/j.spmi.2017.02.002.
29. Delfan A., Liscidini M., and Sipe J. E. - Surface enhanced Raman scattering in the presence of multilayer dielectric structures, J. Opt. Soc. Am. B **29** (2012) 1863-1874. https://doi.org/10.1364/JOSAB.29.001863.
30. Mamichev D. A., Gonchar K. A., Timoshenko V. Y., Mussabek G. K., Nikulin V. E., and Taurbaev T. I. - Enhanced Raman scattering in multilayer structures of porous silicon, J. Raman Spectrosc. **42** (2011) 1392-1395. https://doi.org/10.1002/jrs.2865.
31. Chan S., Kwon S., Koo T. W., Lee L. P., and Berlin A. A. - Surface-Enhanced Raman Scattering of Small Molecules from Silver-Coated Silicon Nanopores, Adv. Mater. **15** (2003) 1595-1598. https://doi.org/10.1002/adma.200305149.
32. Wali L. A., Hasan K. K., and Alwan A. M. - Rapid and Highly Efficient Detection of Ultra-low Concentration of Penicillin G by Gold Nanoparticles/Porous Silicon SERS Active Substrate, Spectrochim. Acta A Mol. Biomol. Spectrosc. **206** (2019) 31-36. https://doi.org/10.1016/j.saa.2018.07.103.
33. Hasi W. L. J., Lin S., Lin X., Lou X. T., Yang F., Lin D. Y., Lu Z. W. - Rapid fabrication of self-assembled interfacial film decorated filter paper as an excellent surface-enhanced Raman scattering substrate. Anal. Methods **6** (2014) 9547-9553. https://doi.org/10.1039/C4AY01775G.
34. Yan Z. X., Zhang Y. L., Wang W., Fu X.Y., Jiang H. B., Liu Y. Q., Verma P., Kawata S., Sun H. B. - Superhydrophobic SERS substrates based on silver-coated reduced graphene oxide gratings prepared by two-beam laser interference. ACS Appl. Mater. Interfaces **7** (2015) 27059-27065. https://doi.org/10.1021/acsami.5b09128.
35. Kundu A., Rani R., Hazra K. S . - Controlled nanofabrication of metal-free SERS substrate on few layered black phosphorus by low power focused laser irradiation. Nanoscale **11** (2019) 16245-16252. https://doi.org/10.1039/C9NR02615K.
36. Lixia Z., Peng L., Lan L., Xiangfeng B., Xiaolei W., Bing Z., Yuan T., - Sensitive Detection of Rhodamine B in Condiments Using SurfaceEnhanced Resonance Raman Scattering (SERRS) Silver Nanowires as Substrate. Appl. Spectrosc. **71** (2017) 2395-2403. https://doi.org/10.1177/0003702817711700.